

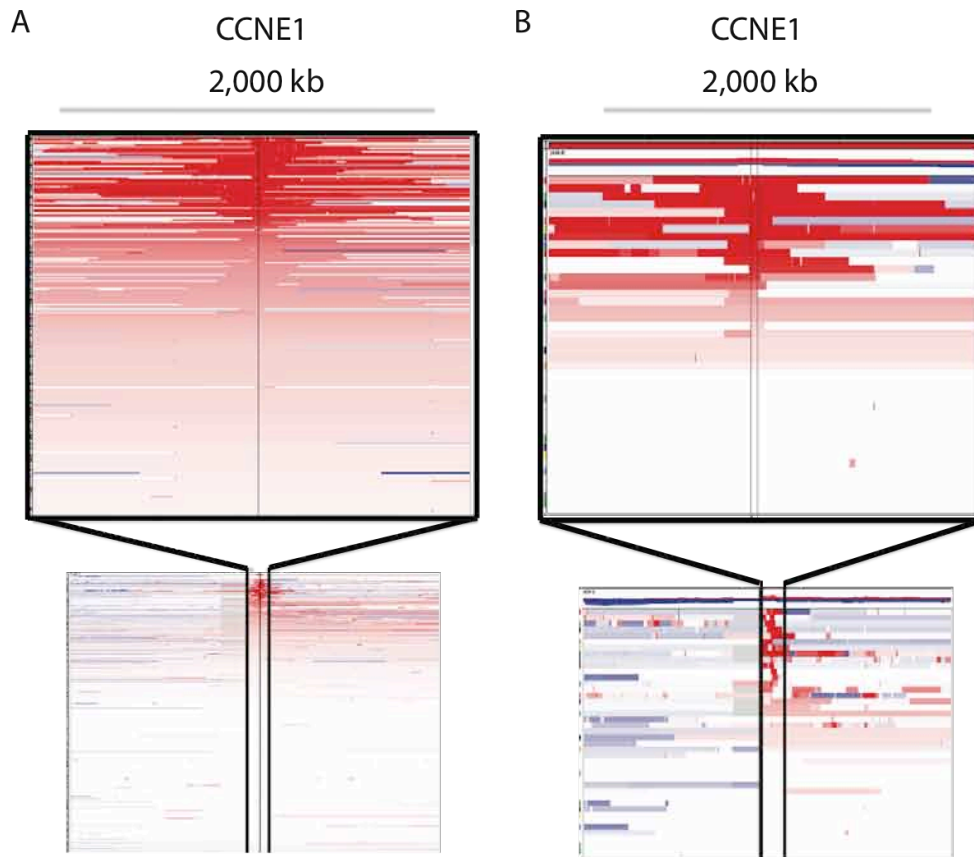
**Supplementary Information For “Pre-existing secondary molecular alterations impact response to ERBB2-directed therapy in *ERBB2*-amplified gastric and esophageal adenocarcinoma”**

**Contents:**

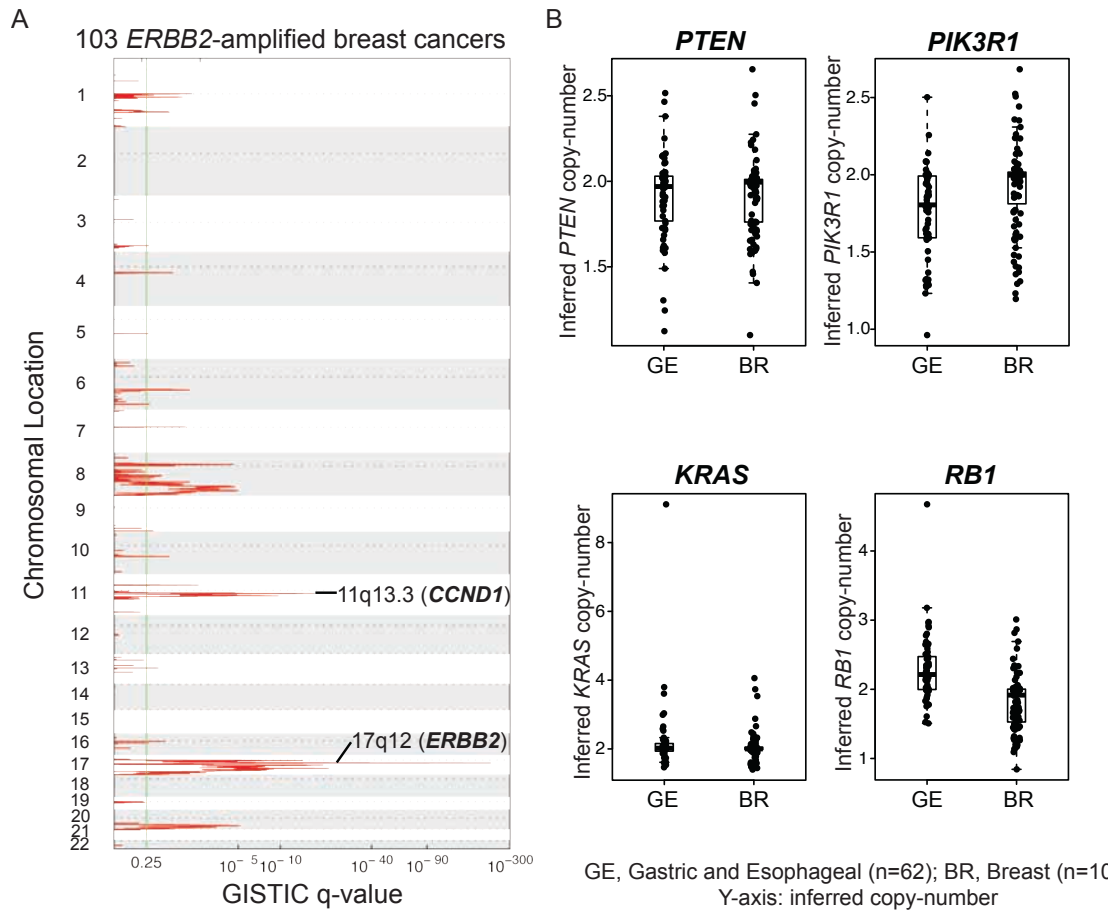
- |   |             |
|---|-------------|
| 1. Supplementary Figures with Legends   | Pages 2-15  |
| 2. Supplementary Methods and References | Pages 16-25 |

Supplementary Tables 1-6 are in separate Microsoft excel files

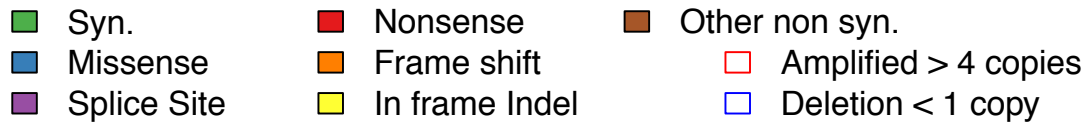
## SUPPLEMENTARY FIGURES



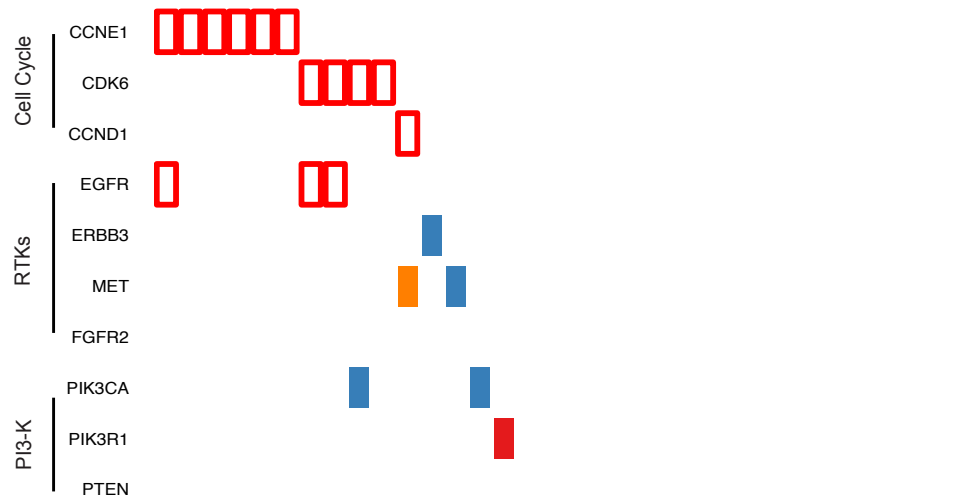
**Supplementary Figure 1.** Integrative Genomics Viewer (IGV) screenshots of chromosome 19p13.3-19q13.45 and the *CCNE1* locus. (A) This overhead view of chromosome 19 shows the focality of *CCNE1* amplification in all 743 gastric/esophageal adenocarcinomas analyzed. (B) This figure shows focal amplifications at the *CCNE1* locus in 62 samples that are also *ERBB2*-amplified. Both of these figures suggest that *CCNE1* amplification is a strongly selected for event and the common amplification of this region is centered on *CCNE1*, as predicted by GISTIC. Two vertical lines at the center of top panels represent the boundary of *CCNE* locus. Red color means copy-number gain and blue color means copy-number loss. (X-axis: chromosomal coordinates; Y-axis: individual cases)



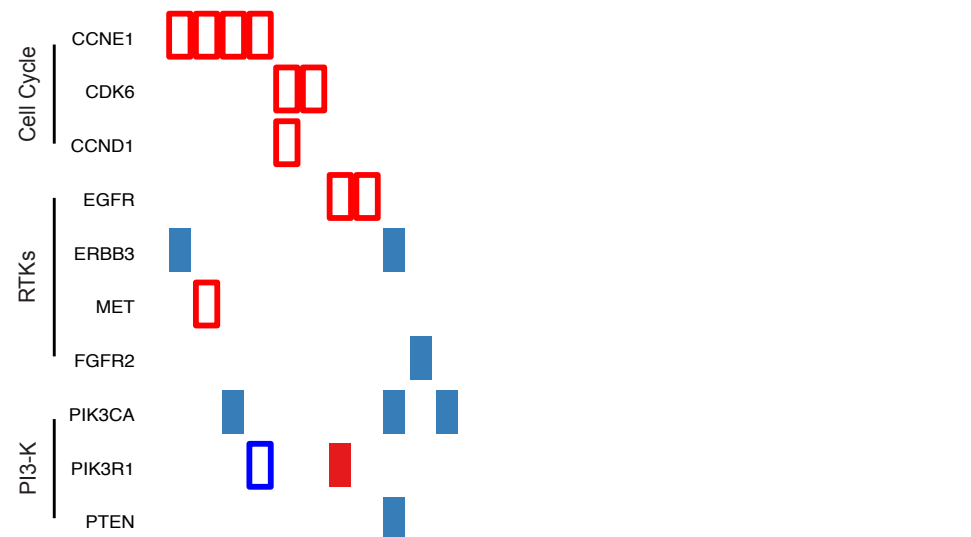
**Supplementary Figure 2.** Co-occurring oncogenic amplifications in *ERBB2*-amplified breast cancer samples. (A) A GISTIC plot for 103 *ERBB2*-amplified breast cancers (x-axis: corrected q-value, y-axis: chromosomal coordinates) exhibits several significant focal amplifications two of which contain important oncogenes (annotated on the right column). (B) Estimated copy-numbers of selected tumor-related genes are depicted on *ERBB2*-amplified GE (n=62) and breast (n=103) cancer samples. One GE adenocarcinoma case shows a high level amplification in *KRAS*, and *RB1* copy-number is more preserved in GE adenocarcinoma. Copy-numbers of *PTEN* and *PIK3R1* are comparable between the two tumor types (GE, gastroesophageal; BR, breast, y-axis: estimated copy-number value).



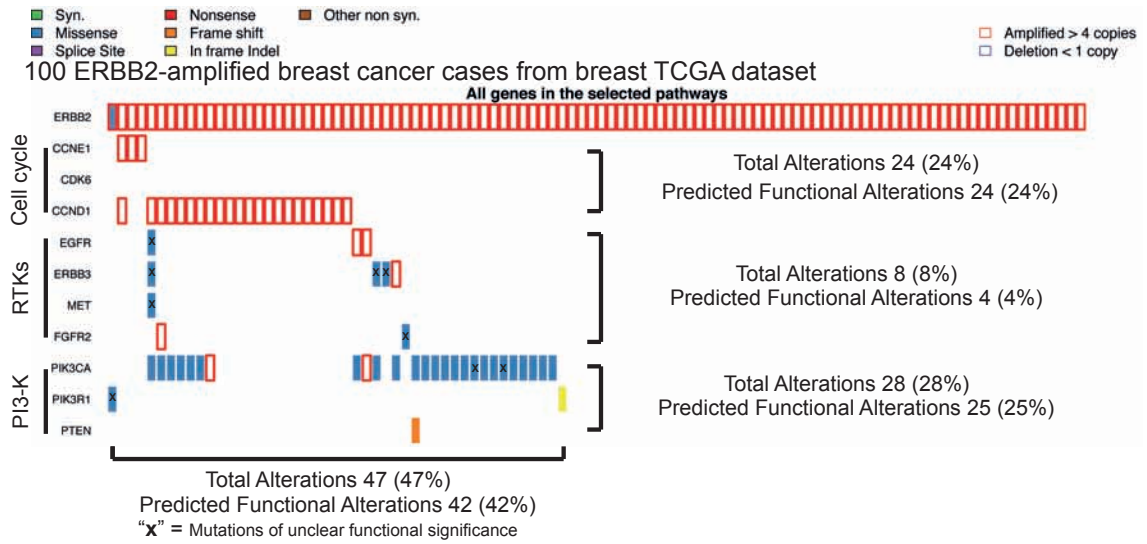
**A** 22 ERBB2-amplified esophageal adenocarcinoma cases with matched whole exome sequencing and copy-number data



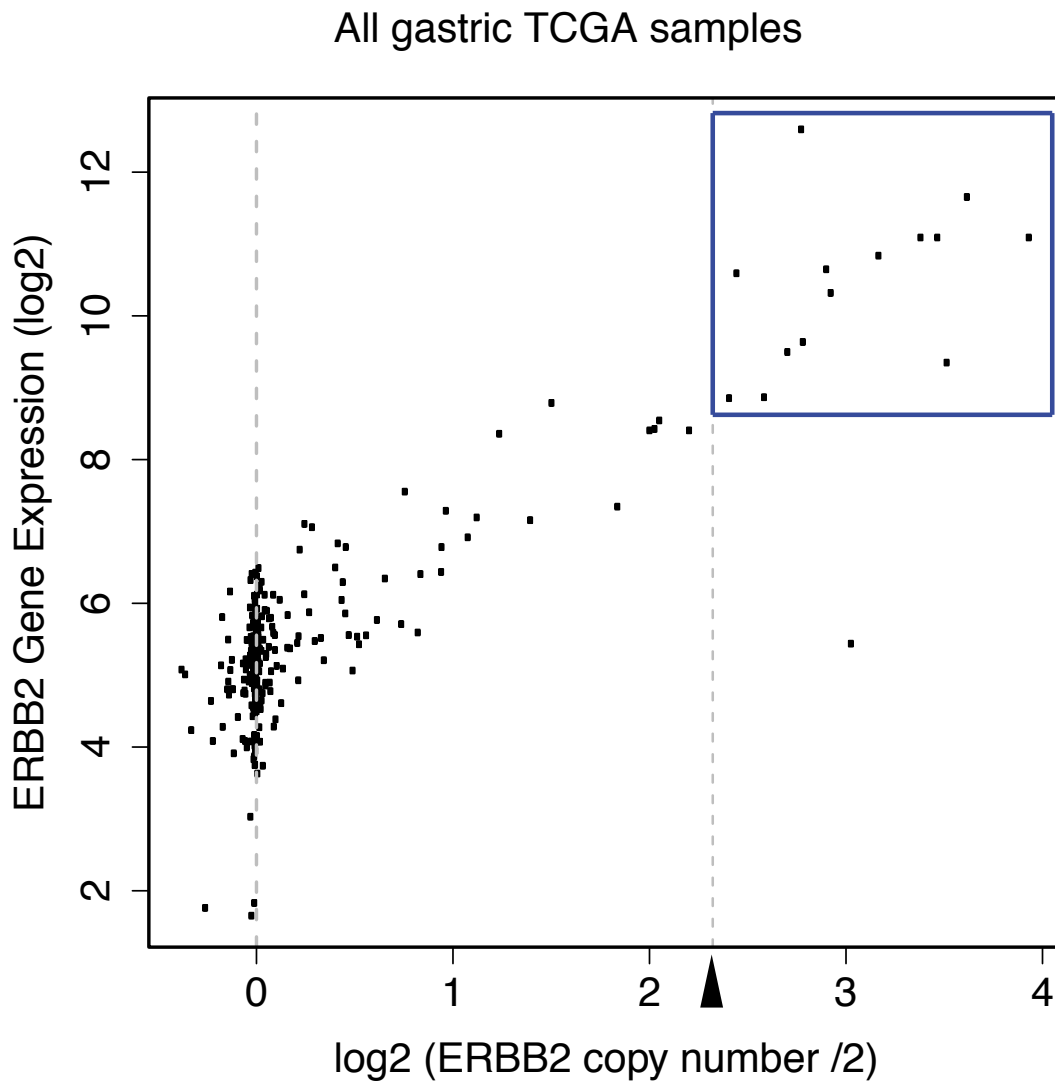
**B** 20 ERBB2-amplified gastric adenocarcinoma cases with matched whole exome sequencing and copy-number data



**Supplementary Figure 3.** An integrated view of co-occurring potentially actionable oncogenic events in 42 HER2+ GE adenocarcinomas broken down into separate 22 esophageal (A) and 20 gastric cases (B). Frequencies of co-occurring oncogenic events are similar between both tumors. X-axis represents individual case and Y-axis represents selected oncogenes. The legend for each event is displayed on the top.

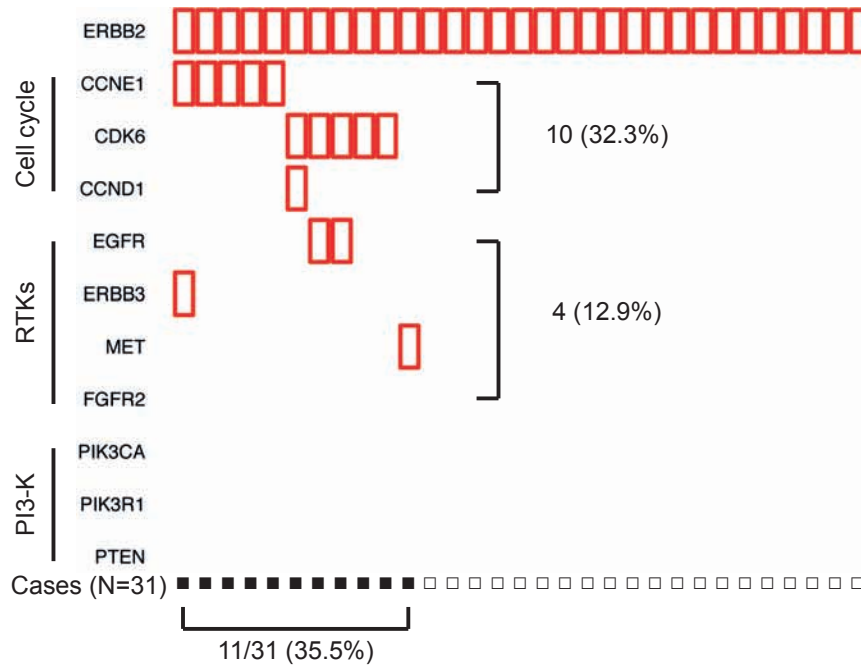


**Supplementary Figure 4.** Integrated view of co-occurring genomic alterations in 100 *ERBB2*-amplified breast cancer cases from TCGA dataset. Each column denotes an individual tumor, and each row displays a gene. Mutations are color coded by the type of each mutation and amplifications are depicted as red outlines. Mutations of unclear functional significance are marked with "x". Predicted activating secondary genomic events are a little bit fewer than those of *ERBB2*-amplified GE adenocarcinoma cases.

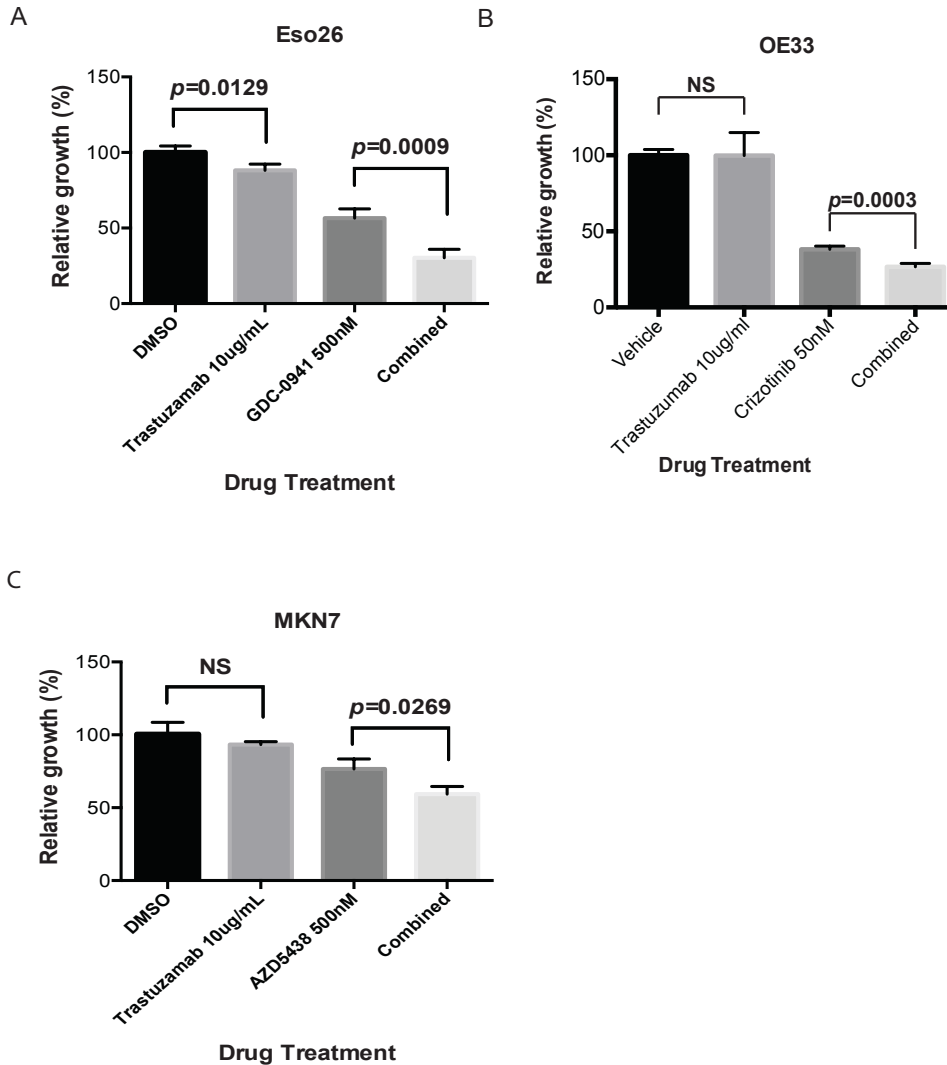


**Supplementary Figure 5.** Scatter plot of all gastric TCGA samples showing the positive correlation between *ERBB2* copy-number and *ERBB2* mRNA expression. Arrowhead represents estimated copy-number of 10. Cases in the dark blue box show that cases with 10+ *ERBB2* copy-number express high level *ERBB2* messages. There is one outlier below the blue box.

31 Gastric and esophageal adenocarcinoma cases with high level of ERBB2 amplification (>10 estimated copy number)

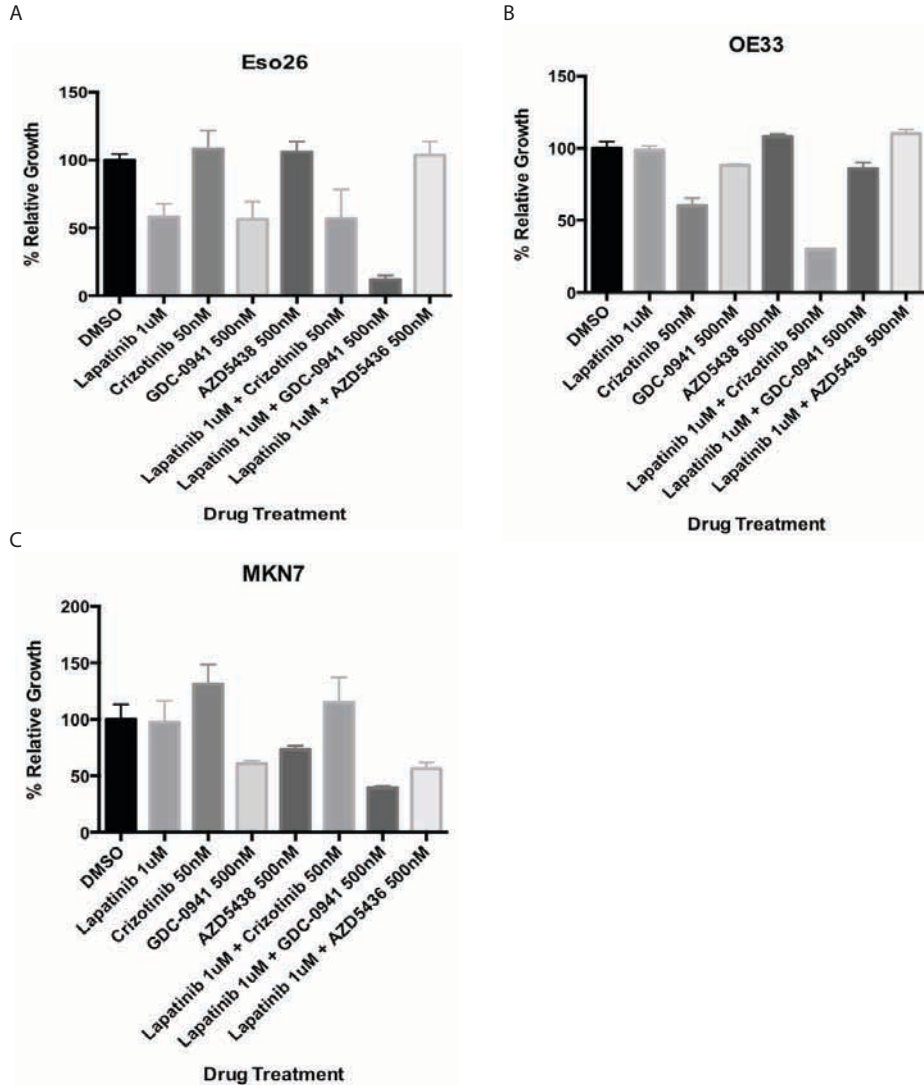


**Supplementary Figure 6.** Secondary oncogenic amplifications in 31 GE adenocarcinoma cases with estimated copy-number of more than 10. X-axis represents individual case and Y-axis represents selected oncogenes. Considerable proportion of GE adenocarcinoma cases with high level of ERBB2-amplification shows secondary oncogenic amplifications. Amplification events are depicted with red boxes.

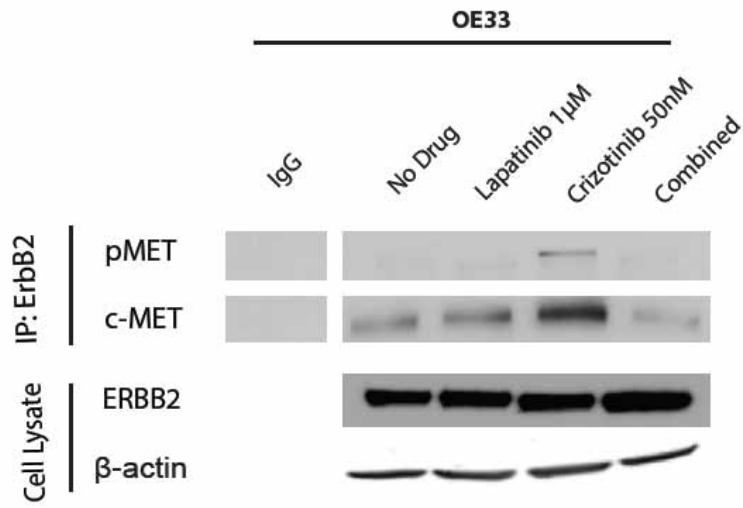


(p-values by t-test)

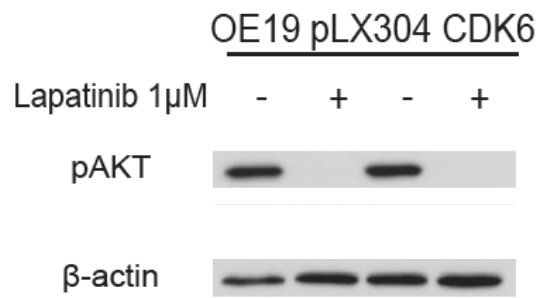
**Supplementary Figure 7.** *In vitro* growth inhibition of ESO26 cells, OE33, and MKN7 cells by targeting ERBB2 and major co-occurring oncogenic events either alone or in combination. (A) ESO26 cells, which have endogenous *PIK3CA* mutation (Q546H) together with *ERBB2* amplification, shows a significant growth inhibition effect on the trastuzumab and GDC-0941 combination treatment while treatment with trastuzumab only has little effect. (B) OE33 cells, which have endogenous *MET* / *ERBB2* co-amplification, show significant growth inhibition on trastuzumab and crizotinib in combination. Trastuzumab alone has no growth inhibitory effect. (C) MKN7, an *ERBB2* amplified cell line that also harbors a *CCNE1* amplification and *PTEN* deletion shows no growth inhibition in the presence of trastuzumab alone. When AZD5438, a CDK2 inhibitor, is added to trastuzumab, there is an enhanced inhibition of cell growth. X-axis shows drug treatment and y-axis shows the relative cell viability compared to vehicle treated control.



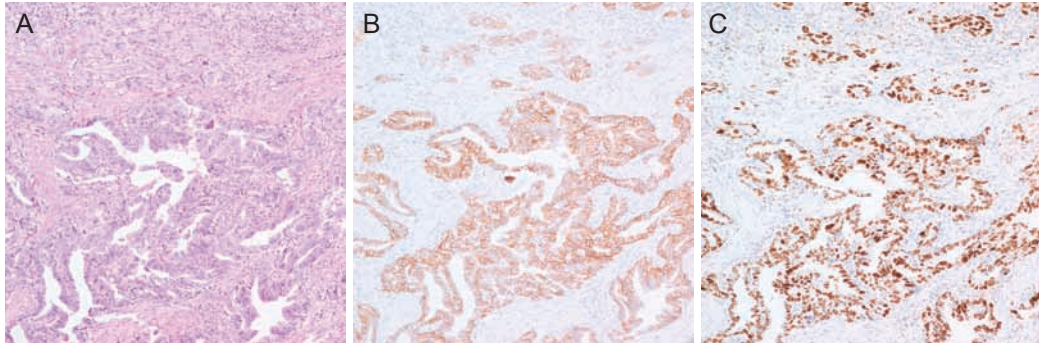
**Supplementary Figure 8.** *In vitro* growth inhibition of ESO26 cells, OE33 cells, and MKN7 cells by using a ERBB2 inhibitor (lapatinib) and other targeted inhibitors of PI3K (GDC-0941), MET (crizotinib), or CDK2 (AZD5438) alone or in combination to demonstrate a specific toxicity of the agents only in cells that harbor alterations in the pathway targeted by the drugs. (A) ESO26, which is *ERBB2* amplified and *PIK3CA* mutant, shows the greatest amount of inhibition when drugs targeting both these alterations are given in combination and no toxicity with the other inhibitors. The column labeled lapatinib+GDC-0941 demonstrates this. (B) OE33, which harbors an amplification of both *ERBB2* and *MET*, shows a strongly synergistic effect on growth inhibition when both ERBB2 and MET are targeted in combination while other targeted agents, either alone or in combination, have little to no effect. This is shown in the lapatinib+crizotinib column. (C) MKN7, an *ERBB2* and *CCNE1* co-amplified cell line that also harbors a *PTEN* deletion, shows increased growth inhibition when lapatinib is added to either AZD5438 or GDC-0941 but not crizotinib. This suggested that both the cell cycle and PI3K axes are important to the viability of these cells. X-axis shows drug treatment and y-axis shows the relative cell viability compared to vehicle treated control.



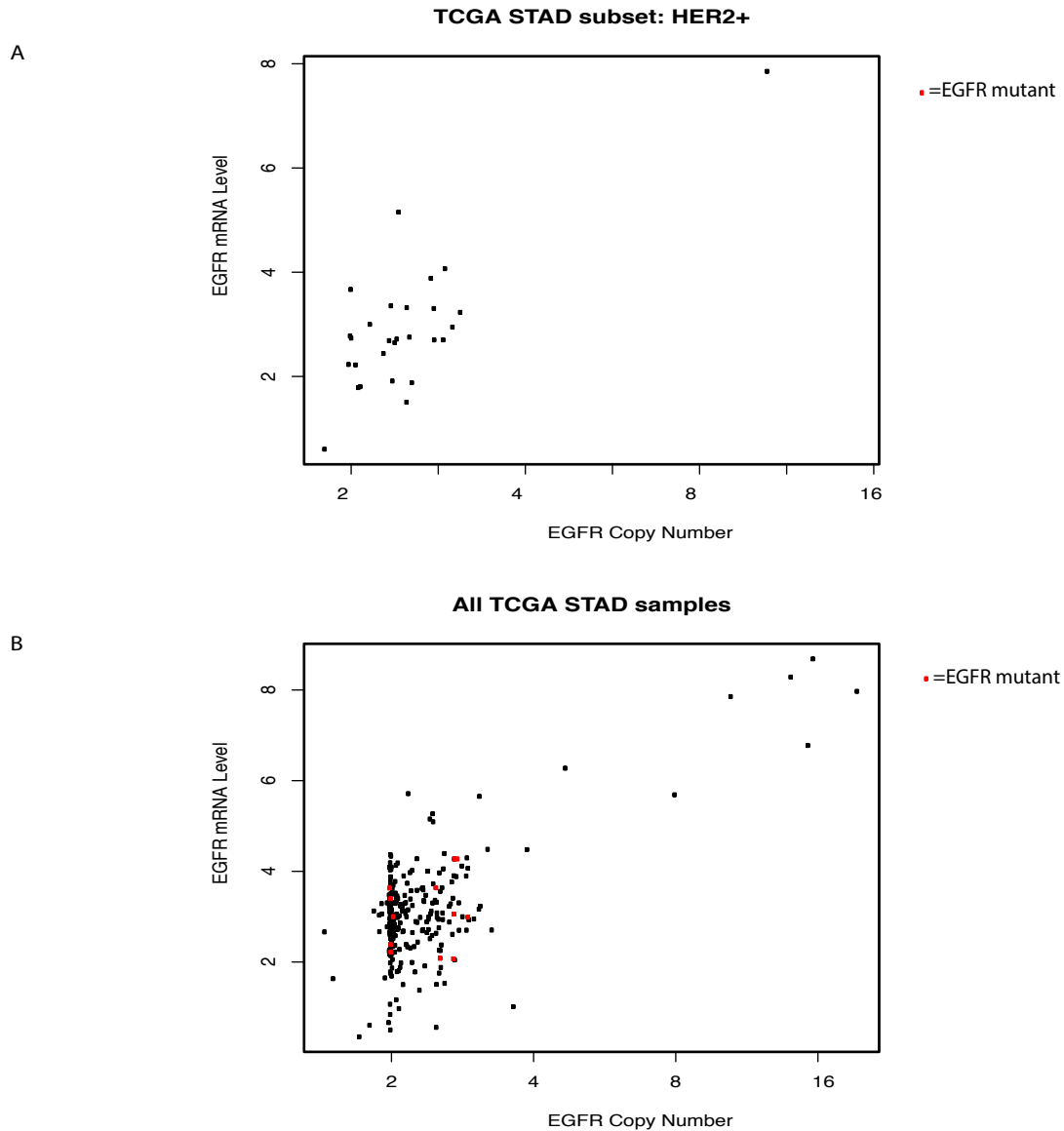
**Supplementary Figure 9.** Immunoprecipitation experiment showing the interaction of ERBB2 and MET in OE33 cells with and without drug treatment. Cell lysates were immunoprecipitated with an anti-ERBB2 antibody then immunoblotted with anti-phospho MET Y1234/1235 and anti-MET antibodies. It is noted that in the presence of crizotinib, the ERBB2:MET dimer increases in abundance and phospho-MET is detected. This suggests a possible compensation mechanism in which ERBB2 attempts to activate MET through dimerization when the major MET signaling is lost but this is only speculation. This observation will require further inquiry to understand.



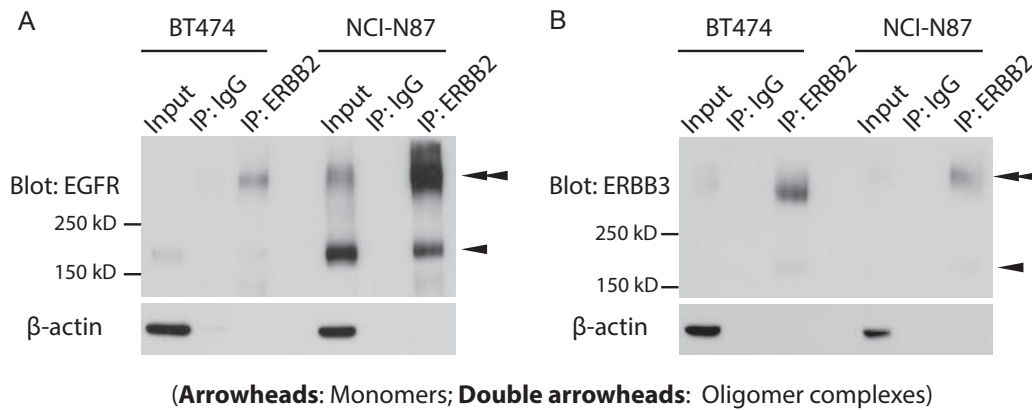
**Supplementary Figure 10.** Phosphorylation status of AKT in OE19 infected with either empty pLX304 vector (left two bands) or pLX304-CDK6 vector (right two bands). Exogenous overexpression of CDK6 did not affect AKT phosphorylation regardless of lapatinib treatment. All proteins were harvested 1 hour after either vehicle or lapatinib treatment.



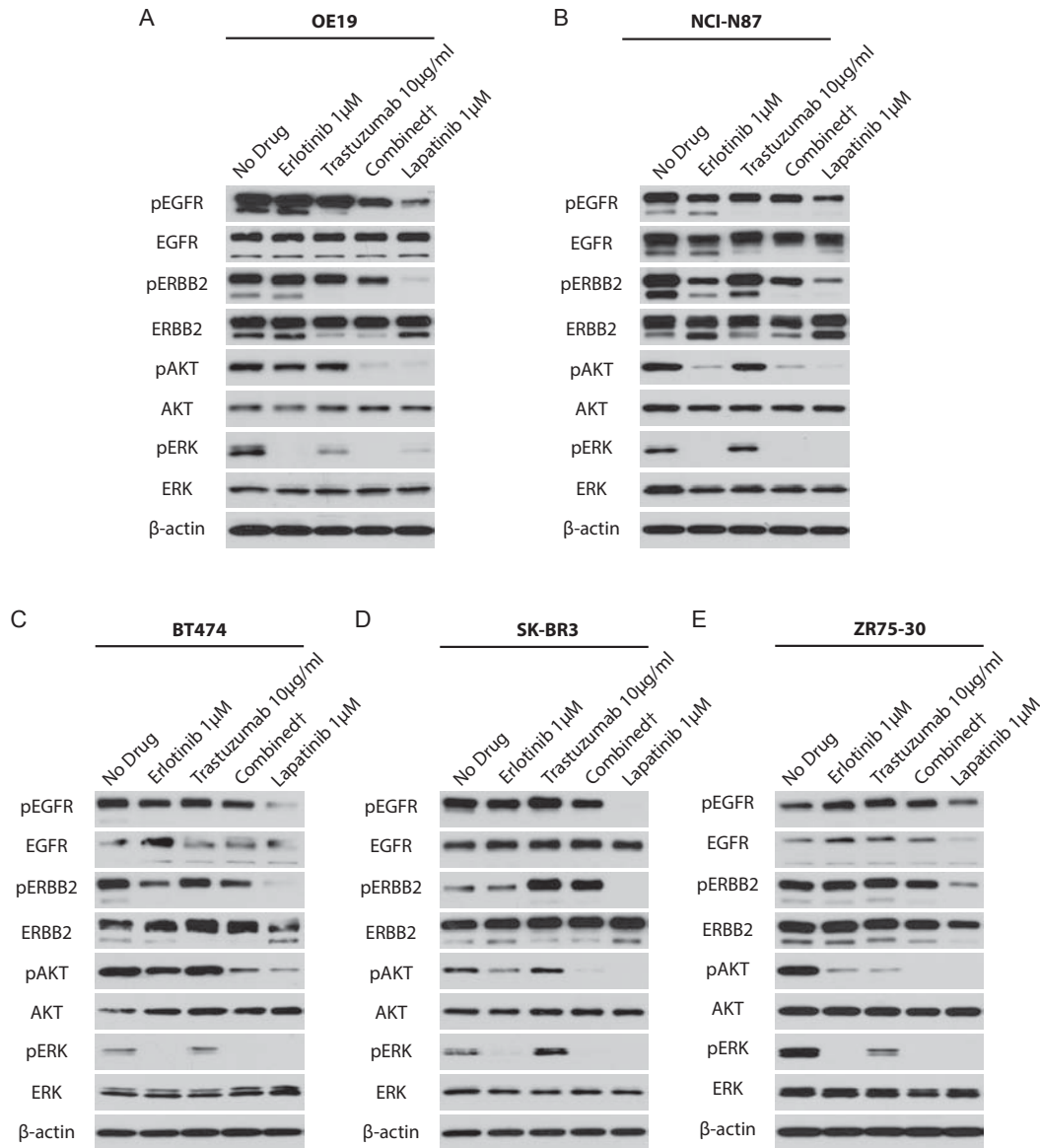
**Supplementary Figure 11.** Immunohistochemistry for ERBB2 and CCNE1 on the same tumor tissue section. (A) Microscopic appearance of a gastric adenocarcinoma case (H&E,  $\times 40$  objective lens). (B) Immunohistochemistry with anti-ERBB2 antibody shows a diffuse strong membranous staining ( $\times 100$  objective lens). (C) Immunohistochemistry with anti-CCNE1 antibody shows a strong nuclear staining in the same tumor cells with ERBB2 protein expression ( $\times 100$  objective lens).



**Supplementary Figure 12.** Scatter plots of *EGFR* copy-number and *EGFR* mRNA expression in 31 *ERBB2*-amplified (A) and all 293 (B) gastric TCGA samples. (A) It is noted that no *EGFR* mutants are seen but increased expression at the mRNA level is observed in *ERBB2*-amplified subset. (B) The plot shows all 293 STAD samples including the 13 samples that are *EGFR* mutant. (X-axis: estimated *EGFR* copy-number; Y-axis: normalized *EGFR* mRNA level in  $\log_2(1+RPKM)$  scale; Red dots: cases harboring *EGFR* mutation)



**Supplementary Figure 13.** Immunoprecipitations and western blots showing the extent of EGFR:ERBB2 (A) or ERBB3:ERBB2 (B) interactions between EGFR-high (NCI-N87) and EGFR-low (BT474) *ERBB2*-amplified cancer cell lines. Cells were seeded at desired densities ( $1.5 \times 10^6$  for NCI-N87,  $3 \times 10^6$  for BT474 in 60 mm dishes). After 24 hours, proteins were crosslinked in tissue culture plate with BS<sup>3</sup>, harvested and were immunoprecipitated with anti-ERBB2 antibody. Immunoprecipitates were immunoblotted with anti-EGFR or anti-ERBB3 antibodies. A small proportion (1/10) of immunoprecipitation input was immunoblotted for comparison together with  $\beta$ -actin loading control.



(†Combined: Erlotinib 1µM + Trastuzumab 10µg/ml)

**Supplementary Figure 14.** Western blots showing the biochemical responses of several *ERBB2*-amplified GE adenocarcinoma and breast cancer cell lines with various levels of EGFR expression to trastuzumab, erlotinib, and the combination of both. Lapatinib-treated cells are also shown for comparison. For erlotinib and lapatinib, proteins were harvested 1 hour after treatment with each drug. For trastuzumab, proteins were harvested 24 hours after treatment. For erlotinib and trastuzumab combination, cells were treated with trastuzumab first and were allowed to grow for 24 hours. Then, erlotinib was added to the culture 1 hour prior to protein harvest. EGFR-high GE adenocarcinoma cell lines (A, B) shows more striking inhibition of EGFR/ERBB2 and AKT phosphorylation on combined trastuzumab and erlotinib treatment, compared to trastuzumab only treatment, than EGFR-low breast cancer cells (C, E). EGFR-high breast cancer cell, SK-BR3 (D) exhibits rebound activation of ERBB2 upon trastuzumab treatment.

## SUPPLEMENTARY METHODS

### **Genomic Analysis of Human Tumor Data**

To interrogate the significantly co-occurring oncogenic copy-number alterations in *ERBB2*-amplified cancers, we took 743 gastric cancer samples with Affymetrix SNP6 data from the published dataset (1, 2) and from those publically available through The Cancer Genome Atlas (TCGA) (3). Sources of datasets are as follows: 1) Dulak AM et al. (1) and Deng N et al. (2): Gene Expression Omnibus (accession no. GSE36460, URL: <http://www.ncbi.nlm.nih.gov/geo/query/acc.cgi?acc=GSE36460>; accession no. GSE31168, URL: <http://www.ncbi.nlm.nih.gov/geo/query/acc.cgi?acc=GSE31168>), 3) Gastric TCGA (3): Primary and processed data, URL: <https://tcga-data.nci.nih.gov/tcga/tcgaDownload.jsp>; Primary sequence files, URL: <https://cghub.ucsc.edu/>; Sample lists, and supporting data, URL: [https://tcga-data.nci.nih.gov/docs/publications/stad\\_2014/](https://tcga-data.nci.nih.gov/docs/publications/stad_2014/)). Among them, we identified 62 *ERBB2*-amplified cases (~8.3% of the dataset) by the criteria that normalized  $\log_2$  (copy-number ratio of tumor / normal) is 0.9 or greater in Affymetrix SNP6 platform. As a  $\log_2$  ratio of 0.9 corresponds to an *ERBB2* copy number of 3.7 (assuming a baseline diploid genome), this threshold approximates the 4-copy cut-off used in standard diagnostic use. (However, the clinical test utilizes fluorescent in situ hybridization and thus only scores tumor cells. By contrast, our genomically-derived data are derived from a combination of tumor and non-tumor DNA and thus leading to attenuation of the *ERBB2* amplification signal from diploid germline DNA. By using the same criterion, we identified 103 *ERBB2*-amplified breast cancer cases (~11.2%) out of 916 patients (4). Then, we ran

GISTIC 2.0 (5) on the Affymetrix SNP6 data of each sample set as described previously (1). We considered focal amplifications with False Discovery Rate q-value  $<0.01$  as statistically significant.

To identify co-occurring mutation, we selected 42 *ERBB2*-amplified GE adenocarcinoma cases from the 486 GE adenocarcinomas with available whole exome sequencing data from our prior study (6) or from TCGA for breast cancer and 103 *ERBB2*-amplified breast cancers from the 916 breast cancer cases with available exome sequencing data (4). For the dataset with whole exome data but without Affymetrix SNP6 data (6), we inferred copy-number profiles from sequencing data using CapSeg algorithm (7). We investigated how many cases had oncogenic mutations in selected cancer-related genes including *PIK3A*, *PIK3R1*, *PTEN*, *CDK6*, *CCND1*, *CCNE1*, *EGFR*, *ERBB2*, *ERBB3*, *MET*, and *FGFR2*.

To evaluate the relative expression of *ERBB3* and *EGFR* across a population of *ERBB2*-amplified breast and GE adenocarcinomas, we queried RNA expression profiling data from gastric and breast TCGA datasets (3, 4). *ERBB2*-amplified cases were defined with the same criteria describe above. The RPKM values were normalized and  $\log_2(1+RPKM)$  values were compared between the two groups.

### **Genomic Characterization of Patient Derived Tissue Samples**

We experienced a particular patient with metastatic *ERBB2*-amplified gastric adenocarcinoma who achieved partial response to combination of

trastuzumab/capecitabine/cisplatin and subsequently progressed during trastuzumab treatment. The presence of *ERBB2* amplification in this case was confirmed by fluorescence in situ hybridization as described previously (8). Fresh frozen tissue samples were obtained from initial gastric biopsy, liver metastasis. The presence and percentage of tumor cells were checked by an experienced pathologist (K.K.). Informed consent was obtained before tissue harvest and this protocol was approved by the Institutional Review Board at the Samsung Medical Center. All samples were shipped to the Center for Cancer Genome Discovery at the Dana Farber and all analyses have been done thereafter. For genomic characterization, we used a focused Illumina exome capture sequencing platform as described previously (9).

### **Cell Lines and Reagents**

OE19 and NCI-N87 cells were obtained from the European Collection of Cell Culture (ECACC) and the American Type Culture Collection (ATCC) respectively. OE33 cells were purchased from the Sigma (St. Louis, MO) and MKN7 cells were obtained from the JCRB Cell Bank. KYAE1, ESO26, OACM5.1C, OACP4C, and SKGT4 cells were provided by Tony Godfrey and BT474, SK-BR3, and BT474 cells were provided by William Hahn. SK-BR3 cells were maintained in McCoy's 5A medium (Mediatech, Inc., Manassas, VA) supplemented with 10% fetal bovine serum (FBS) (Gemini Bio-Products, West Sacramento, CA) and Penicillin/Streptomycin/L-Glutamine (P/S/G). All other cells were maintained in RPMI1640 medium (Mediatech, Inc., Manassas, VA) supplemented with 10% FBS and PSG. All cells were kept in a humidified incubator at 5% CO<sub>2</sub>. Small molecule inhibitors such as lapatinib, NVP-BEZ235, GDC-0941, and crizotinib were

purchased from the LC laboratories and trastuzumab was purchased from the Department of Pharmacy at the Dana-Farber Cancer Institute. NVP-BEZ235 was dissolved in dimethylformamide and all other small molecule inhibitors were dissolved in dimethylsulfoxide (DMSO).

### **Vectors and Retroviral Infection**

pBabe-HA-PIK3CA E545K (Addgene #12525) and H1047R (Addgene #12524) and pBabe-Flag-myristoylated AKT1 (Addgene #15294) were obtained from Addgene ([www.addgene.org](http://www.addgene.org)). pLX304-CDK6 lentiviral vector was made from pDONR223-CDK6 (Addgene #23688) by performing LR clonase reaction with pLX304 destination vector according to manufacturer's instructions (Invitrogen). This lentiviral vector has V5 tag on the C-terminus of CDK6 open reading frame enabling the usage of anti-V5 antibody to check the CDK6 protein expression. Viral production and target cell infection were performed as described previously (10). Retroviruses containing each construct were produced by transfecting early-passage 293T cells ( $4 \times 10^6$  per each virus) with 3 $\mu$ g pCL-Ampho and 3 $\mu$ g of each construct in the presence of FuGENE transfection reagent (Promega). Lentiviruses were produced by transfecting 293T cells with 300ng VSVG, 2.7 $\mu$ g delta-8.9 and 3 $\mu$ g each construct. Target cells were infected with each virus in the presence of polybrene (8 $\mu$ g/ml) for 6 hours. Eighteen hours later, the infected target cells were selected by culturing them in 1.5 $\mu$ g/ml puromycin for 7 days before biological experiments. Cells infected with pLX304-CDK6 were selected with 3 $\mu$ g/ml blasticidin.

### ***In vitro* drug sensitivity assay**

We used Cell-titer Glo assay (Promega) to measure cell viability. Briefly, cells were plated at a desired density onto 96-well plate. After 24 hours, cells were treated with either vehicle or variable doses of small molecule inhibitors and then allowed them to grow for 3 days. For trastuzumab, cells were grown 5 days after treatment. Then, the relative amount of ATP was measured by Cell-titer Glo luminescence assay according to manufacturer's instructions.

### **Protein crosslinking and Immunoprecipitation**

To detect oligomerized ERBB family member proteins, we crosslinked protein in cultured cells as described previously with slight modification (11). Briefly, cells were seeded at a desired density in 60 mm culture plate ( $1.5 \times 10^6$  for NCI-N87 cells and  $3 \times 10^6$  for BT474 cells). Twenty-four hours later, cells were rinsed with HEPES buffer (150mM NaCl, 25mM HEPES). Then, BS<sup>3</sup> (bis(sulfosuccinimidyl) suberate) (Peirce) was added to cells at a final concentration of 1mM and incubated on a rocking platform for 30 minutes at room temperature. Crosslinking reaction was quenched by the addition of Tris-HCl pH7.5 to a final concentration of 20mM. After crosslinking, cells were harvested with Triton X-100 lysis buffer (1% Triton X-100, 50mM Tris-HCl pH 7.5, 135mM NaCl, 1mM EDTA pH 8.0, 1mM EGTA pH 8.0, 2.5mM sodium pyrophosphate, and 10mM  $\beta$ -glycerophosphate) supplemented by protease inhibitor cocktail (Roche) and phosphatase inhibitor cocktails (Calbiochem). One milligram of cell lysate was divided into two tubes and each of them was immunoprecipitated with 1 $\mu$ g of control rabbit IgG (sc-2027, Santa Cruz Biotechnology) or anti-ERBB2 (Clone e2-4001, Thermo Scientific)

antibody conjugated to 25µl of protein A/Sepharose beads (Invitrogen) overnight at 4°C. The mixture was washed three times with PBS and boiled for 5 minutes in 20µl of 2× loading buffer before being subjected to SDS-polyacrylamide gel electrophoresis.

### **Western blotting**

Cells were lysed with RIPA lysis buffer (50mM Tris-HCl pH 7.5, 150mM NaCl, 0.1% SDS, 1% NP-40, 0.5% sodium deoxycholate) supplemented by protease inhibitor cocktail (Roche) and phosphatase inhibitor cocktails (Calbiochem). Lysates were separated on 4-12% Tris-Glycine SDS-polyacrylamide gel and were transferred to PVDF membranes (Millipore). The membranes were blocked with 5% skim milk (Bio-Rad) dissolved in TBST buffer (50mM Tris-HCl, 150mM NaCl, 0.05% Tween-20). Then, the membranes were incubated with primary antibodies overnight at 4°C. Anti-EGFR antibody (#A300-388A) was purchased from Bethyl Laboratories, anti-ERBB3 antibody (#sc-285) from Santa Cruz Biotechnology and anti-phospho-tyrosine antibody (clone 4G10, #05-321) from Millipore. Anti-β-actin antibody (#A5441) was purchased from Sigma-Aldrich. All other antibodies including anti-phospho EGFR Y1068 (#3777), anti-phospho ERBB2 Y1221/1222 (#2243), anti-ERBB2 (#2165), anti-phospho-ERK (#4370), anti-ERK (#4695), anti-phospho AKT S473 (#4060), anti-AKT, anti-phospho ERBB3 Y1289 (#4791), anti-phospho MET Y1234/1235 (#3077), anti-MET (#8198) and anti-cyclin E1 (#4129) were purchased from Cell Signaling Technologies. Horseradish peroxidase-conjugated secondary antibodies (anti-rabbit: #31460, anti-mouse: #31430, Pierce) and SuperSignal West Pico Chemiluminescent Substrate (Pierce) were used to detect signals.

### **Tissue microarray and Immunohistochemistry**

To evaluate the relative frequency of EGFR expression in *ERBB2*-amplified GE adenocarcinomas and in breast cancers, we used tissue microarray that had matched copy-number information. The tissue microarray sets for GE adenocarcinoma and breast cancer were provided by Z.Z. and P.T., respectively. We confirmed *ERBB2* overexpression/amplification by immunohistochemistry and chromogen in situ hybridization (CISH) as described previously (12). For immunohistochemistry for EGFR, we stained sections of tissue microarray with anti-EGFR antibody (Clone 2-18C9) (DAKO, Carpinteria, CA). Briefly, antigens in de-paraffinated and rehydrated tissue microarray sections were retrieved by heating sections in 99°C water bath for 40 minutes. After endogenous peroxidase activity was quenched and nonspecific binding was blocked, primary antibody was incubated at room temperature for 30 minutes. The secondary antibody (Flex HRP) was allowed to incubate for 30 minutes. After washing, sections were incubated with Flex 3,3'-diaminobenzidine for 10 minutes and counterstained with Flex Hematoxylin for 5 minutes. Archived human placental tissue served as positive control. Negative control staining was performed by replacing anti-EGFR antibody with normal serum. EGFR stained tissue microarray slides were reviewed by Z.Z. and P.T. EGFR staining was considered positive when more than 10% of the stained tumor cells showed unequivocal membranous staining.

To address the intra-tumor heterogeneity in terms of *ERBB2* and *CCNE1* overexpression in the *ERBB2*-amplified GE adenocarcinoma, we performed immunohistochemistry for *ERBB2* and *CCNE1* on a collection of 23 human gastric cancers with strong (3+) *ERBB2*

expression where four distinct sites were available for testing. We stained them with anti-ERBB2 (Novocastra, Newcastle, UK) and anti-CCNE1 (ThermoFisher Scientific, USA, clone HE12) antibodies. Signals were detected with polymer-based DAKO Envision detection system. All staining procedures were done by using VENTANA autostainer.

### **Patient-derived tumor cells and drug treatment**

Malignant cells were isolated from malignant ascites drained for therapeutic purposes after obtaining informed consent form. The protocol was approved by the Institutional Review Board at Samsung Medical Center. The cells were cultured in RPMI media supplemented with 10% fetal bovine serum. Briefly, cells ( $3 \times 10^3$  in 100  $\mu$ L/well) were seeded on 96-well plates and incubated for 24 h at 37°C and treated with drugs (lapatinib or AZD5438) for 3 d at 37°C. After drug treatment, MTS solution was added to each well and incubation was continued for 4 h at 37°C. Absorbance value of each well was measured with a microplate reader set at 490 nm. All experiments were performed in triplicates.

### SUPPLEMENTARY METHOD REFERENCES

1. Dulak AM, Schumacher SE, van Lieshout J, Imamura Y, Fox C, Shim B, Ramos AH, Saksena G, Baca SC, Baselga J, et al. Gastrointestinal Adenocarcinomas of the Esophagus, Stomach, and Colon Exhibit Distinct Patterns of Genome Instability and Oncogenesis. *Cancer Res.* 2012;72(17):4383-93.

2. Deng N, Goh LK, Wang H, Das K, Tao J, Tan IB, Zhang S, Lee M, Wu J, Lim KH, et al. A comprehensive survey of genomic alterations in gastric cancer reveals systematic patterns of molecular exclusivity and co-occurrence among distinct therapeutic targets. *Gut*. 2012;61(5):673-84.
3. Comprehensive molecular characterization of gastric adenocarcinoma. *Nature*. 2014.
4. Comprehensive molecular portraits of human breast tumours. *Nature*. 2012;490(7418):61-70.
5. Mermel CH, Schumacher SE, Hill B, Meyerson ML, Beroukhi R, and Getz G. GISTIC2.0 facilitates sensitive and confident localization of the targets of focal somatic copy-number alteration in human cancers. *Genome Biol*. 2011;12(4):R41.
6. Dulak AM, Stojanov P, Peng S, Lawrence MS, Fox C, Stewart C, Bandla S, Imamura Y, Schumacher SE, Shefler E, et al. Exome and whole-genome sequencing of esophageal adenocarcinoma identifies recurrent driver events and mutational complexity. *Nat Genet*. 2013;45(5):478-86.
7. Pugh TJ, Weeraratne SD, Archer TC, Pomeranz Krummel DA, Auclair D, Bochicchio J, Carneiro MO, Carter SL, Cibulskis K, Erlich RL, et al. Medulloblastoma exome sequencing uncovers subtype-specific somatic mutations. *Nature*. 2012;488(7409):106-10.
8. Cho EY, Srivastava A, Park K, Kim J, Lee MH, Do I, Lee J, Kim KM, Sohn TS, Kang WK, et al. Comparison of four immunohistochemical tests and FISH for measuring HER2 expression in gastric carcinomas. *Pathology*. 2012;44(3):216-20.

9. Wagle N, Berger MF, Davis MJ, Blumenstiel B, Defelice M, Pochanard P, Ducar M, Van Hummelen P, Macconail LE, Hahn WC, et al. High-throughput detection of actionable genomic alterations in clinical tumor samples by targeted, massively parallel sequencing. *Cancer Discov.* 2012;2(1):82-93.
10. . The RNAi Consortium. <http://www.broadinstitute.org/rnai/trc>.
11. Penuel E, Akita RW, and Sliwkowski MX. Identification of a region within the ErbB2/HER2 intracellular domain that is necessary for ligand-independent association. *J Biol Chem.* 2002;277(32):28468-73.
12. Hu Y, Bandla S, Godfrey TE, Tan D, Luketich JD, Pennathur A, Qiu X, Hicks DG, Peters JH, and Zhou Z. HER2 amplification, overexpression and score criteria in esophageal adenocarcinoma. *Mod Pathol.* 2011;24(7):899-907.